Journal of Applied Sciences

ISSN 1812-5654

science alert

ANSInet
an open access publisher
http://ansinet.com

Journal of Applied Sciences 9 (9): 1752-1757, 2009
ISSN 1812-5654

Optimization of a Detector Collimator for Use in a Gamma-Ray Backscattering Device for Anti-Personal Landmines Detection

H. Tavakoli-Anbaran, H. Miri-Hakimabad and R. Izadi-Najafabadi
Department of Physics, Faculty of Sciences, Ferdowsi University of Mashhad, Mashhad, Iran

Abstract: In the present study, a new detector collimator has been designed to detect the buried anti-personal (AP) landmines for use in gamma-ray backscattering device, with Monte Carlo method. The new detector collimator is made by lead and it has the cylindrical shape with 11.2 mm in height, 12.6 mm in inner radius, 13.3 mm in outer radius and 0.7 mm in thickness of the shielding layers around detector. The mass of the designed detector collimator is also 7.24 g.

Key words: Compton scattering, detector shield, different shapes of collimator, explosive materials detection, MCNP code

INTRODUCTION

The search for hidden explosive is one of the most interesting and worthwhile applications of nuclear techniques. In particular, Compton scattering of photons from isotopic gamma sources have been employed. In this way, explosive material could be detected by consideration of Compton cross-section dependence on both electron and mass density. Nitrogen-based explosives have density in the range from 1650 to 1900 kg m^{-3} (Hussein, 1992) which makes them lighter than most of metals, but heavier than common materials and different in density from various types of soil. Therefore, density can be used to detect the presence of landmine (Hussein and Waller, 1998). The use of Compton scattering in the detection of landmine was first investigated by the US Army in 1970s (Roder and Konyneburg, 1975). Isotopic sources were utilized to take advantage of their small size, light weight, self-powered nature and low-cost. A portable device was developed using a ^{241}Am source along with a small scintillation detector and an associated audio alarm system. Tang and Hussein (2004) also re-examine the utility of sources ^{60}Co, ^{137}Cs, ^{192}Ir and ^{241}Am for the detection of shallowly buried AP landmines. Then ^{241}Am source was selected as the photon source for subsequent simulation and also for experimental study. In this study, the new detector collimator (its shape and dimensions) was obtained.

MONTE CARLO SIMULATION

The well-known MCNP code was applied to perform the calculations in this study. MCNP is a general purpose, three dimensional general geometry, time dependent, Monte Carlo N Particle code that is used to calculate coupled neutron-photon-electron transport. For photon, the code accounts for incoherent and coherent scattering, the possibility of fluorescent emission after photoelectric absorption, absorption in pair production with local emission of annihilation radiation and bremsstrahlung.

The results of Monte Carlo simulations are analyzed considering four indicators: (1) the magnitude of the backscattering photon flux (ϕ); (2) the difference between the detector response obtained in the presence of a target and that obtained in target-free soil, normalized to that of target-free soil to define a contrast ratio, (C); (3) the shape of the change of the detector response with detector position (the contrast trend) and (4) in term of a figure-of-merit (fom) defined as fom = $\phi \times c$. Good detection capability was defined by the ability to obtain a contrast ratio grater than 10% while uncertainty in simulation results was required to be lower than 5%. A high flux reduce the required counting time and/or source strength (hence shielding requirements and device weight), while a high contrast shows good distinction ability between materials. Therefore, an optimized device should provide simultaneously a high flux and contrast, i.e., a high value of fom. To optimize a gamma-ray backscattering system we should also attend to two points: (1) isolation of detector from direct exposure to source radiation and (2) focusing the detector's filed-of-view on the region of interest.

The first point dose here, using a well-collimated photon source (20 mm in diameter of beam of photon) in Monte Carlo simulation as evident in Fig. 1 and as such no source radiation is allowed to reach the detector, but

Corresponding Author: Hossien Tavakoli Anbaran, Department of Physics, Faculty of Physics, Shahrood University of Technology, Shahrood, Iran
Tel: +98-273 3332205-9 2658 Fax: +98-273 3335270

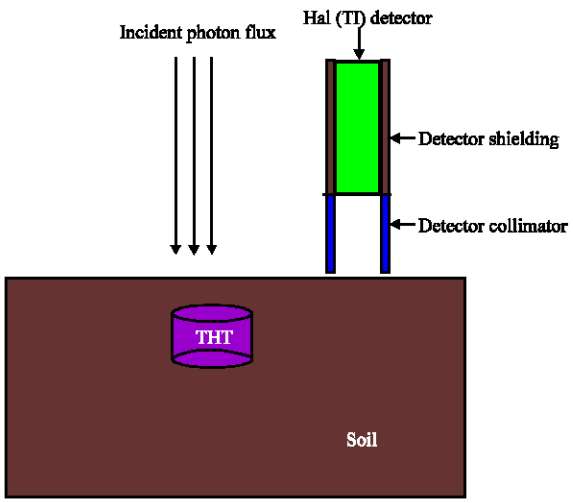

Fig. 1: The diagram of simulated geometry

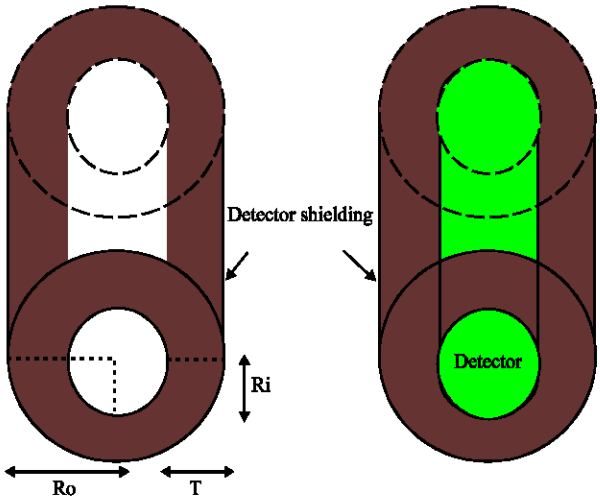

Fig. 2: The diagram of detector shielding without detector and with detector

leakage of source radiation to the detector is a factor in experimental works that we should attend to it. Although, we use a well-collimated photon source in Monte Carlo simulation we can use those Monte Carlo results in experimental works, because the Half-Value-Layer (HVL) of lead at source energy of 60 keV equals to 0.14 mm, therefore if the source is shielded for example with 10 mm in thickness of lead i.e., the thickness of lead shielding is about 71 HVL's, radiation reaching the detector from radiation source would have been attenuated by a factor of $2^{71} = 2.3\times10^{21}$.

The second point dose here, using both the detector shielding and the detector collimator. To obtain the above earlier indicators, we use MCNP code, in the case that Tang and Hussein's (2004) setup have the best contrast, i.e., the buried landmine have 100 mm in radius, 160 mm in height, 10 mm in depth-of-burial and 100 mm in detector-distance from center of source.

SIMULATION OF THE DETECTOR SHIELDING

To simulate the detector shielding, a lead cylindrical with both inner radius (Ri) equal to the inner radius of the NaI(Tl) detector and outer varied radius (Ro) was written in MCNP code input-file. The diagram of the detector shielding is shown in Fig. 2. To obtain the best thickness of the detector shielding (i.e., determining the ability of the system to increase the contrast and the fom), the thickness of the detector shielding was varied from 0.0 to 200 $D_{1/2}$. Therefore, we can determine the thickness of the detector shielding from the equation bellow:

$$t = Ro\text{-}Ri = nD_{1/2} \quad (1)$$

where, n is the natural number from 0 to 200 and $D_{1/2}$ is the half-value-layer of lead at source energy of 60 keV equals to 0.14 mm. Note that we need to run MCNP code for the different thicknesses of the detector shielding; therefore we should estimate a thickness to increase the detector shielding thickness in each step of MCNP code running. We can add each thickness to increase the detector shielding thickness, but we should attend to two points: (1) if the increased thickness to the detector shielding is the large amount, it may cause that we can not see the real maximum or minimum points of the contrast and (2) if the increased thickness to the detector shielding is the small amount, it may cause that the time of MCNP code running is the large amount because of increasing the amount of n in the Eq. 1, therefore we think that the best estimated thickness in each step of MCNP code running is $D_{1/2}$. For this reason, to exchange the radius, height and thickness of the detector shielding or the detector collimator, in each step of MCNP code running, we use $D_{1/2}$.

Figure 3 and 4 show that maximum contrast value gave 5 $D_{1/2}$ in the thickness of the detector shielding and fom values are increasing with increasing the thickness of the detector shielding because of gamma rays back scattering in the detector shielding, so it is caused to increase the weight of the system, therefore the best thickness of the detector shielding is 5 $D_{1/2}$.

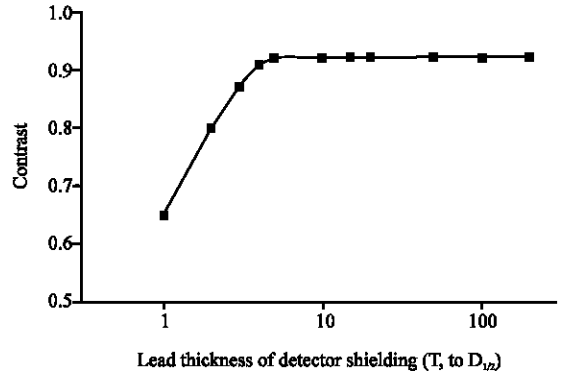

Fig. 3: Plot of contrast versus lead thickness of detector shielding

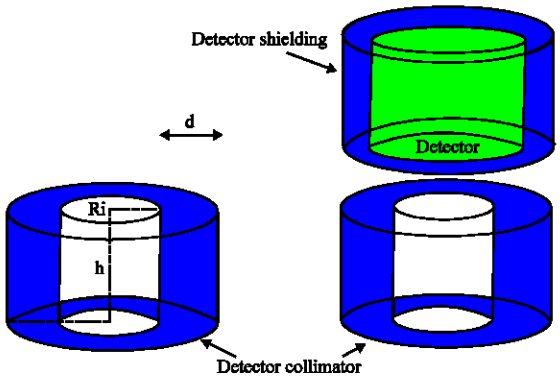

Fig. 5: The diagram of detector collimator without detector and with detector

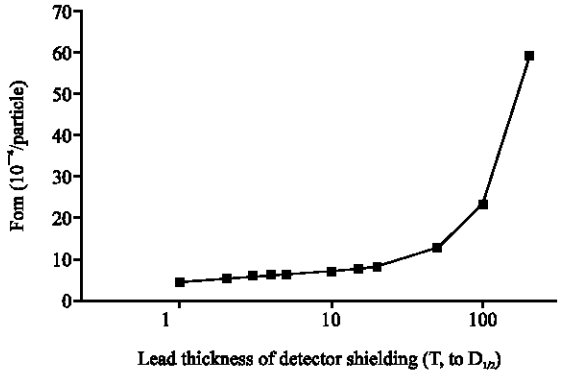

Fig. 4: Plot of fom versus lead thickness of detector shielding

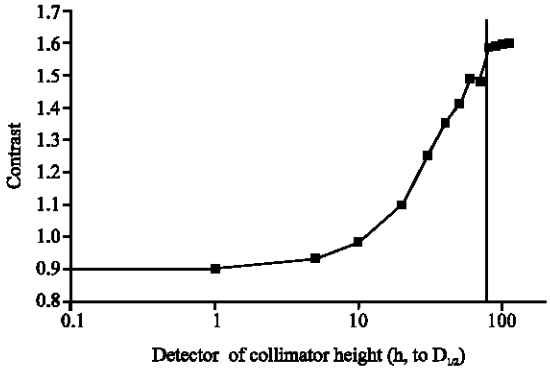

Fig. 6: Plot of contrast versus height of detector collimator

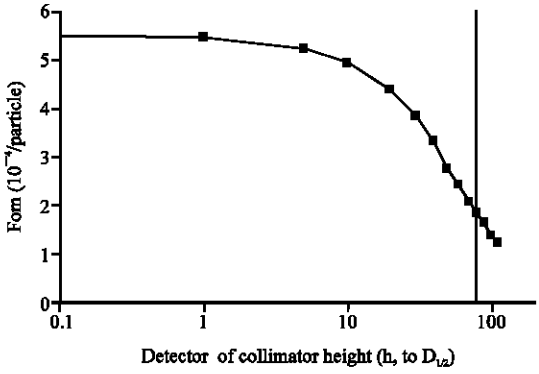

Fig. 7: Plot of fom versus detector collimator height

SIMULATION OF DETECTOR COLLIMATOR AND IT'S DIFFERENT SHAPES

For this purpose, at first, we assumed a cylindrical detector collimator with inner radius (Ri) equal to the inner radius of the NaI(Tl) detector and 5 $D_{1/2}$ in its thickness (d) i.e., equal to the thickness of the detector shielding. The height of detector collimator (h) was also varied from 0.0 to 110 $D_{1/2}$. Then in each step of MCNP code running, an integer number multiple of $D_{1/2}$ was increased to the detector collimator height to determine the best detector collimator height. The diagram of the detector collimator is shown in Fig. 5-7 show that maximum contrast value gave 80 $D_{1/2}$ in height and fom values are decreasing with increasing height detector collimator because of decreasing the detector's field-of-view as compared to without the detector collimator case. For the best height of the detector collimator, the inner radius of detector collimator (Ri) was varied from 0.0 to 90 $D_{1/2}$ (the NaI(Tl) detector radius) like it was down for the detector collimator height. Figure 8 and 9 show that maximum contrast value gave 90 $D_{1/2}$ in inner radius and fom values are increasing with increasing inner radius of the detector collimator because of increasing the detector's field-of-view with increasing the detector collimator inner radius. We also considered that the shape of the detector collimator was a defective cone (diverging and converging collimator) with 5 $D_{1/2}$ in thickness (d), 80 $D_{1/2}$ in height (h), 90 $D_{1/2}$ in inner radius of the top surface (R) (i.e., it must equal to the NaI(Tl) detector radius because of increasing Compton backscattering gamma-ray beams

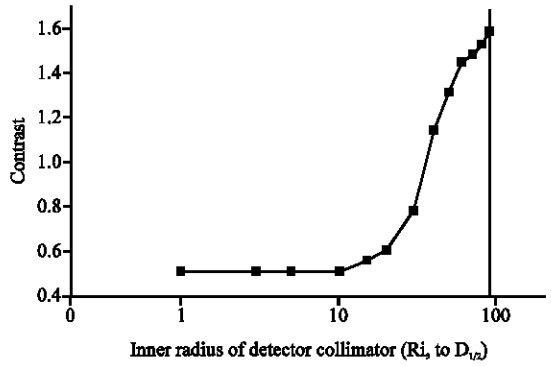

Fig. 8: Plot of contrast versus inner radius of detector collimator

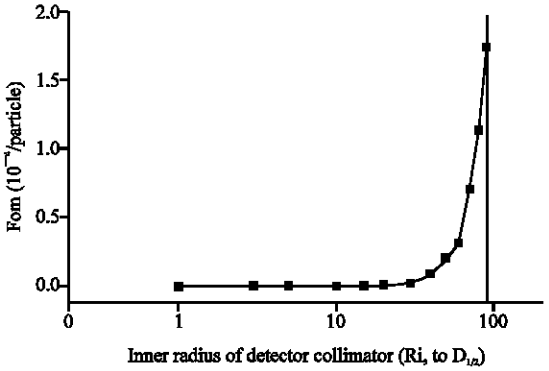

Fig. 9: Plot of fom versus inner radius of detector collimator

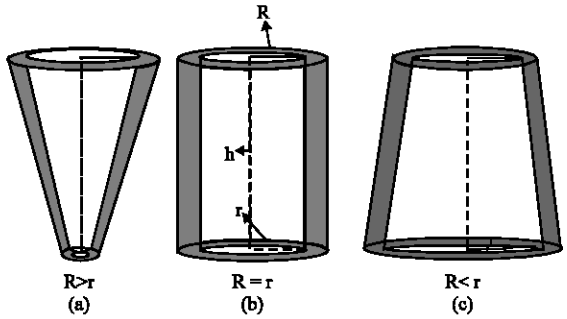

Fig. 10: The diagram of the three types of detector collimator shapes

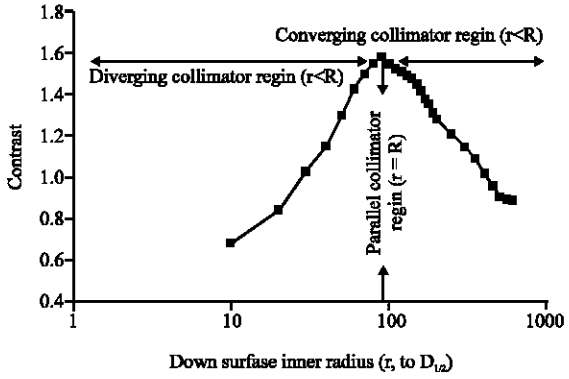

Fig. 11: Plot of contrast versus down surface inner radius of detector collimator (r) with defective cone shape. The diverging or converging collimator is, respectively obtain when the inner radius of the down surface (r) lower or larger than the inner radius of the top surface (R). Also, the parallel collimator is obtain when the inner radius of the down surface (r) equals to the inner radius of the top surface (R)

are reached directly to the window of the detector to increase fom) and inner radius of down surface (r) was varied from 0.0 to 600 $D_{1/2}$. The geometry of the three types of the detector collimator shapes has been shown in Fig. 10. Attend to this point, the down surface inner radius was only changed to obtain the three types of the defective cone, i.e., we can, respectively obtain the diverging and converging collimator with changing down surface inner radius from 0.0 to 89 $D_{1/2}$ and from 91 $D_{1/2}$ to 600 $D_{1/2}$ and if the down surface inner radius is equal to 90 $D_{1/2}$, we obtain the parallel collimator. Figure 11 shows that maximum contrast value gave 90 $D_{1/2}$ in inner radius of the down surface. Therefore, the novel detector collimator has the cylindrical shape. From simulating above, we also deduced that there is not any benefit in using a two-stage collimator (diverging towards the soil, then converging towards the detector, or vice versa) because if the two-stage collimator is used, the detector's field-of-view increases or decreases in compared to case which is used the parallel collimator. When the detector's field-of-view increases, the fom also increases and the contrast decreases, because the contrast has only the maximum value for the parallel collimator or the detector's field-of-view decreases, both the fom and the contrast decreases, because the contrast has only the maximum value for the parallel collimator.

USING THE DESIGNED COLLIMATOR FOR ANTI-PERSONAL LANDMINES DETECTION

After obtaining the shape and the size of the detector collimator and the best thickness of the detector shielding, they are used to detect Anti-Personal (AP) landmines. For this purpose we obtain the maximum depth-of-burial of AP landmines with the new detector collimator. The contrast of TNT versus the depth-of-burial of AP landmine was obtained. According to what was

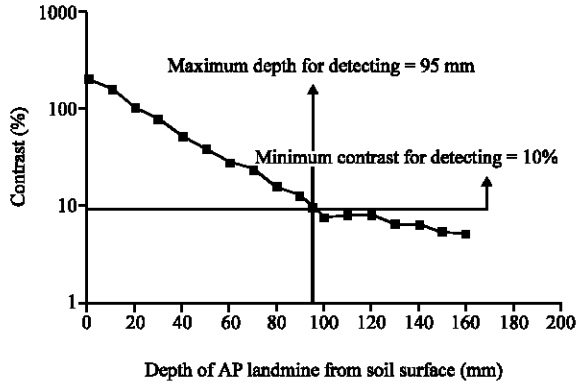

Fig. 12: Plot of contrast versus depth-of-burial of AP landmine with the best detector collimator for heavy TNT

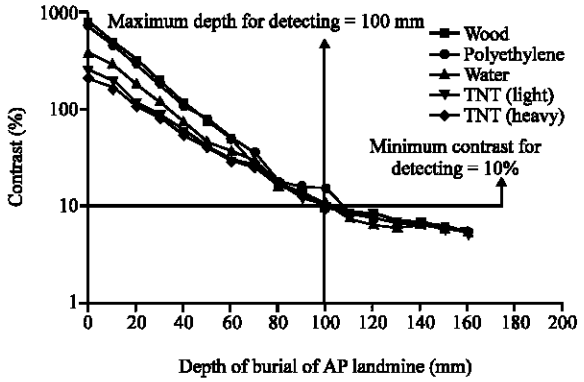

Fig. 13: Plot of contrast versus depth-of-burial of AP landmine for the five different materials

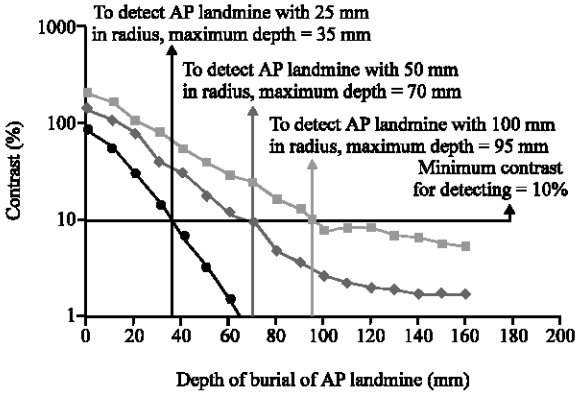

Fig. 14: Plot of contrast versus depth-of-burial of AP landmine for the heavy TNT. There are the three different sizes in AP landmine radius (25, 50 and 100 mm)

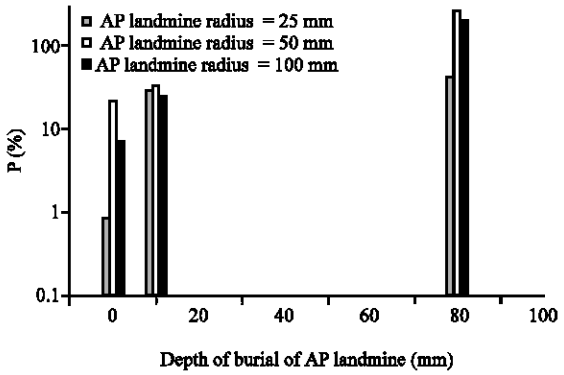

Fig. 15: Plot of P versus the depth-of-burial of AP landmine for heavy TNT. There are the AP landmines with the three different radiuses (25, 50 and 100 mm)

shown in Fig. 12, the maximum depth-of-burial of AP landmines equals 95 mm. Also Fig. 13 shows the contrast in some materials (Hussein *et al*., 2005). According to the Fig. 13, we show that there are considerable differences between the contrast of TNT (light or heavy) with the contrast of other materials (wood, polyethylene and water) from 0.0 to 100 mm in the depth-of-burial of AP landmine. At the end, over works were down for two different types of the AP landmines with 50 and 25 mm in radius. Figure 14 shows their results for the maximum depth-of-burial of AP landmine. According to Fig. 14, the maximum depth-of-burial of AP landmines decreases with decreasing the radius of AP landmines. Using the new detector collimator, the contrast for each of the materials (Hussein *et al*., 2005) were obtained. Also the difference between the contrast obtained in the presence of the new detector collimator and that obtained in the detector collimator of Tang and Hussein's (2004) setup, normalized to that of obtained in the detector collimator of Tang and Hussein's (2004) setup, multiplied by 100 (it defines P) were calculated for all the materials. Figure 15 shows the amounts of P for heavy TNT with the three different radius of AP landmines (25, 50 and 100 mm) and the three different depth-of-burial of AP landmines (0, 10, 80 mm).

RESULTS AND CONCLUSION

As for the Monte Carlo simulations the following are perceived:

- The novel detector collimator has the cylindrical shape with 80 $D_{1/2}$ = 11.2 mm in height, 90 $D_{1/2}$ = 12.6 mm in inner radius, 95 $D_{1/2}$ = 13.3 mm in outer radius therefore 5 $D_{1/2}$ = 0.7 mm in thickness of lead

- The novel detector shielding has the cylindrical shape with inner radius equals to NaI(Tl) detector radius and the thickness equals to 5 $D_{1/2}$
- By the novel detector collimator, the heavy TNT contrast (with the depth-of-burial equals to 10 mm) increases about 25% for landmines as small as 100 mm in radius, 33% for them 50 mm in radius and 28% for them 25 mm in radius (Fig. 15)
- By increasing the depth-of-burial of AP landmines, the heavy TNT P increases for each of the three radiuses (Fig. 15) so the effect of the novel detector collimator can be observed better
- The depth-of-burial of AP landmines increases about 25% for landmines as small as 100 mm in radius (Fig. 14), 55% for them 50 mm in radius and 40% for them 25 mm in radius
- The contrast is increased by the novel detector collimator for each of the materials (Hussein *et al*., 2005) (Fig. 13)

At the end, the detector collimator and the detector shielding which was designed in this investigation can be used in each gamma-ray backscattering device which use from ^{241}Am source to measure like what we did. With designing such collimator, the fom has the maximum value that it might obtain, because the collimator window equals to the NaI(Tl) detector window and it can be caused that the time of count considerably decreases. It can also be said that detector collimator plays an important role in detecting the AP landmines as a special situation and contrast, fom and the depth-of-burial of AP landmine can be increased interestingly by the novel detector collimator.

REFERENCES

Hussein, E.M.A., 1992. Detection of Explosive Materials using Nuclear Radiation: A Critical Review. In: Aviation Security Problems and Related technologies: Critical Review of Optical Science and technology, Makky, W.H. (Ed.). SPIE Optical Engineering Press, Bellingham, Washington, pp: 126-136.

Hussein, E.M.A. and E.J. Waller, 1998. Review of one-side approaches to radio-graphic imaging for detection of explosives and narcotics. Radiat. Meas., 29: 581-591.

Hussein, E.M.A., M. Desrosiers and E.J. Waller, 2005. On the use of radiation scattering for the detection of landmines. Radiat. Phys. Chem., 73: 7-19.

Roder, F.L. and R.A. van Konynenburg, 1975. Theory and application of X-ray and gamma-ray backscatter to landmine detection. Technical Report 2134, US Army Mobility Equipment Research and Development Center. http://oai.dtic.mil/oai/oai?verb=getRecordandmetadataPrefix=html and identifier=ADA015541.

Tang, S.S. and E.M.A. Hussein, 2004. Use of isotopic sources for identifying anti-personnel landmines. Applied Radiat. Isotope, 61: 3-10.